This is an open access article published under an ACS AuthorChoice License, which permits copying and redistribution of the article or any adaptations for non-commercial purposes.

Journal of chemical & engineering data

Article

pubs.acs.org/jced

Viscosity and Density of Aqueous Solutions of Carbon Dioxide at Temperatures from (274 to 449) K and at Pressures up to 100 MPa

Mark McBride-Wright, Geoffrey C. Maitland, and J. P. Martin Trusler*

Qatar Carbonates and Carbon Storage Research Centre (QCCSRC), Department of Chemical Engineering, Imperial College London, South Kensington Campus, London SW7 2AZ, United Kingdom

ABSTRACT: The viscosity and density of aqueous solutions of carbon dioxide having mole fractions of CO_2 of 0.0086, 0.0168, and 0.0271 are reported. The measurements were made in the single-phase compressed liquid region at temperatures between (294 and 449) K at pressures up to 100 MPa; additional density measurements were also made at T = 274 K in the same pressure range. The viscosity was measured with a vibrating-wire viscometer while the density was measured by means of a vibrating U-tube densimeter; both were calibrated with pure water and either vacuum or ambient air. The density data have an expanded relative uncertainty of 0.07 % with a coverage factor of 2. From the raw data, the partial molar volume of CO_2 in aqueous solution has been determined and correlated as an empirical function of temperature and pressure. When combined with the IAPWS-95 equation of state of pure water, this correlation represents the measured densities of under-saturated solutions of CO_2 in water within ± 0.04 %. The viscosity data have an expanded relative uncertainty of 1.4 % with a coverage factor of 2. A modified Vogel–Fulcher–Tamman equation was used to correlate the viscosity as a function of temperature, pressure, and mole fraction of CO_2 with an absolute average relative deviation of 0.4 %. The viscosity and density of saturated aqueous solutions of CO_2 may be calculated by combining the correlations presented in this work with a suitable model for the mole fraction of CO_2 at saturation.

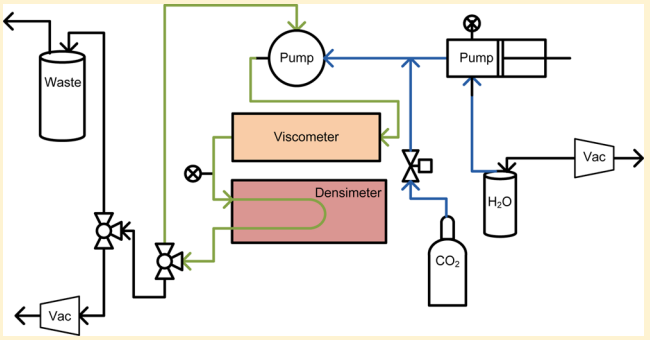

1. INTRODUCTION

Carbon dioxide is a fluid commonly used in the chemical and petroleum industries. It plays an important role in the refrigeration industry as a replacement for chlorofluorocarbons (CFCs) which have high global warming potentials (GWP).[1] It is used as a supercritical fluid in extraction and purification processes and, in environmental engineering, for treatment of industrial waste liquids.[2] It is also used in oilfield process engineering as a fluid for enhanced oil recovery (EOR).[3,4] However, because CO_2 is a greenhouse gas and huge volumes are emitted annually from anthropogenic sources, large-scale capture of CO_2 from fossil fuel combustion processes, and subsequent geological storage, is currently being considered. This process is known as carbon capture and storage (CCS). Deep saline aquifers represent a sink that can potentially store very large amounts of CO_2 on a geological time scale. Consequently, there is interest in the physical and chemical properties of mixtures of CO_2 and water or brine.

Understanding the multiphase flow properties of CO_2 and brines in porous media is essential for successful large-scale geologic CO_2 storage. Optimizing the design and operation of injection projects will depend upon expectations about the distribution of CO_2 in the subsurface, knowledge of injectivity, and estimates of the capacity of permanent trapping processes. It is recognized that the capillarity of the CO_2–brine system in porous media is important in controlling fluid flow over lengths ranging from subcore to basin scale.[5] The distribution of CO_2 in the subsurface, including the column height in contact with the caprock and the surface extent of the plume, is dependent upon capillary pressure–saturation relationships, and the relative permeability function.[6] Small variations in relative permeability can strongly influence injectivity and, in turn, the number of wells required to meet an overall injection goal.[7] Lower-than-expected injectivity is a well-known but poorly understood phenomenon in the CO_2 EOR processes, and may be due to poorly characterized relative permeability functions[8] and/or inaccurate knowledge of fundamental thermophysical properties.

When CO_2 is injected into an aquifer, some of it dissolves in the brine leading to a solution of higher density than the original brine.[9] Natural convection due to negative buoyancy may then lead to the CO_2-dense brine sinking toward the bottom of the reservoir formation at a rate that is influenced by, among other factors, viscosity. This process allows undissolved CO_2 to contact fresh brine and so it accelerates the rate of dissolution thereby shortening the time scale for the storage of CO_2 by solubility trapping.[2] Knowledge of the viscosity and density of the CO_2–brine system is therefore essential in reservoir flow simulations used to model the injection and long-term fate of CO_2 in a storage project. Inspection of the

Received: September 30, 2014
Accepted: December 2, 2014
Published: December 12, 2014

 © 2014 American Chemical Society dx.doi.org/10.1021/je5009125 | J. Chem. Eng. Data 2015, 60, 171–180

Table 1. Available Experimental Data for Viscosity η and Density ρ of (H_2O + CO_2) with Relative Uncertainty U_r at Temperatures T and Pressures p

reference	property	phase	T/K	p/MPa	x_2	U_r
Kumagai et al.[11]	η	L	273 to 278	0.1 to 30	$\leq 1.59\cdot10^{-2}$	1.5 %
Uchida et al.[12]	η	L	273 to 282	0.7 to 5	saturation	2.3 %
Tabasinejad et al.[2]	ρ	G and L	382 to 478	3.5 to 129	saturation	< 0.01 %
Li et al.[10]	ρ	L	332	3.3 to 29	saturation	0.01 %
Hebach et al.[13]	ρ	L	284 to 333	1.0 to 30	saturation	0.15 %
Yaginuma et al.[14]	ρ	G and L	304	1.0 to 10	saturation	0.01 %

literature yields a very limited amount of experimental data for the viscosity and density of solutions of CO_2 in water or brine, especially in relation to high-pressure and high-temperature conditions. Li et al.[10] performed an extensive literature survey considering experimental transport-property data for mixtures with dissolved CO_2.[2,10−14] As summarized in Table 1, the data available for viscosity are sparse, derived from only a few sources, and restricted to low temperatures and relatively modest pressures. The situation for density is slightly better, but the database is still limited.

In our work, we seek to expand substantially the ranges of temperature, pressures, and mole fraction over which the viscosity and density of aqueous solutions of CO_2 are known. We begin in this paper with the (CO_2 + H_2O) binary system because this system is easier to study than the (CO_2 + brine) system and also exhibits the highest solubility of CO_2, thereby maximizing the effect that we wish to study. The effects upon viscosity of dissolved CO_2 and dissolved salts are probably almost separable so that the results of the present study will be transferrable to (CO_2 + brine) systems. The present study on the (CO_2 + H_2O) binary system extends in temperature from 274 K (for density) or 296 K (for viscosity) up to 449 K, with mole fractions of CO_2 up to 0.027, and pressures up to 100 MPa. These ranges of temperature and pressure extend beyond typical aquifer conditions but allow for the construction of a more wide-ranging model.

2. APPARATUS

There are numerous methods available for viscosity and density determination, each of which has their respective benefits. The techniques used in this work for viscosity and density measurements are the vibrating-wire (VW) viscometer and vibrating U-tube (VT) densimeter, respectively. Thus, the experimental system developed is referred to as the VW−VT apparatus. Figure 1 is a schematic diagram of the VW−VT apparatus.

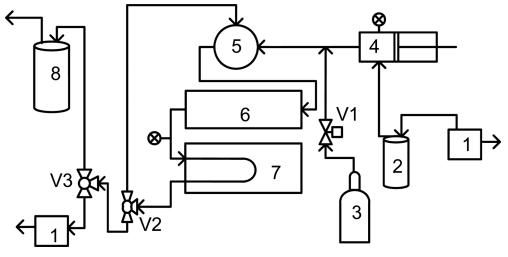

Figure 1. Schematic of VW−VT apparatus: (1) vacuum pump, (2) water reservoir, (3) CO_2 cylinder, (4) syringe pump, (5) circulating pump, (6) vibrating wire viscometer, (7) vibrating tube densimeter, (8) waste, (V1 to V3) valves.

Since the VW−VT apparatus was designed for work with aqueous solutions, including concentrated brines, a high resistance to corrosion was needed. Consequently, wetted parts of the fluid system were made from Hastelloy-C276 (HC-276) as it provides good resistance to corrosion.[15,16]

The VW technique has previously been used successfully to study hydrocarbons with dissolved CO_2.[17] The sensor used in this study was a compact design in which the tensioned vibrating wire is clamped securely at both ends. The absence of a tensioning weight allows the device to be used in any orientation and, like all VW viscometers, it requires no bulk movement of the fluid because it is the wire itself that vibrates.

In the VW technique, the tensioned wire becomes a stiff string through which a sinusoidal alternating current of frequency f is passed thereby generating a transverse force due to the presence of a perpendicular magnetic field. The vibration of the wire induces a voltage proportional to the velocity of the wire in addition to that arising from the passage of the current through the electrical impedance presented by the stationary wire. A lock-in amplifier demodulates, filters, and digitizes the signal to yield the in-phase and quadrature components of the combined complex voltage V. The resonance curve $V(f)$ is represented by a rigorous theoretically derived working equation[18] as follows:

$$V = \frac{\Lambda i f}{f_0^{\,2} - f^2(1+\beta) + i f^2(\beta' + 2\Delta_0)} + a + bi + cif \tag{1}$$

Here, Λ is the amplitude, and f_0 and Δ_0 are the resonance frequency and logarithmic decrement of the wire in vacuum. In eq 1, β and β' are real-valued terms that account for the added mass and damping arising from the fluid around the wire and are given by

$$(\beta' + i\beta) = \frac{\rho}{\rho_s}\left[\frac{i + 4_i K_1(\sqrt{i\Omega})}{\sqrt{i\Omega}\,K_0(\sqrt{i\Omega})}\right] \tag{2}$$

where

$$\Omega = \frac{2\pi f \rho R^2}{\eta} \tag{3}$$

ρ and η are the density and viscosity of the fluid, R and ρ_s are the radius and density of the wire, and K_n is the modified Bessel functions of the second kind with order n. The remaining terms in eq 1 arise from the impedance of the stationary wire.

The wire material should be of high density, high tensile strength, high melting temperature, sufficient hardness, and adequate electrical conductivity. Tungsten, which meets these criteria, has been the material of choice in most previous work. However, we experienced difficulties with tungsten wires in aqueous systems and adopted instead an alloy of platinum and

dx.doi.org/10.1021/je5009125 | J. Chem. Eng. Data 2015, 60, 171−180

iridium containing 90 mass % Pt. The wire used was 0.15 mm in diameter and the density of the material at T = 298.15 K is 21560 kg·m^{-3}.[19]

The viscosity sensor was similar to that described by Peleties and Trusler[20] and comprised a ceramic flow tube with metallic end pieces between which the wire was clamped. These end pieces were made from Monel K-500 and contained pins which were used for aligning the wire along the center line of the flow tube, and clamping plates to hold the wire securely in place under axial tension. The main body of the sensor, made from Shapal-M ceramic, was 52 mm in length, with an outer diameter 11.5 mm and an inner diameter of 6.0 mm. The end pieces were attached using epoxy resin (Stycast 2850 FT cured with catalyst 9) and, when assembled, the length of wire stretched between the end pieces was 50 mm. M2 screws, also made from Monel K-500, were used to hold down the clamping plates for the wire at each end and also for securing one solder tag at each end for the electrical connections. The outer surface of the ceramic tube was machined to accept a pair of O-rings (Kalrez Spectrum 7090, i.d. 9.5 mm × 1 mm section) in 10.0 mm diameter recesses, thereby centering the sensor within the 12.0 mm bore of the pressure vessel. This effectively prevented the metallic end-pieces from touching the inside wall of the vessel and thereby avoided short circuits.

For assembly, with the sensor orientated vertically, a length of wire was passed through, aligned and secured to the top clamp, and tensioned by attaching a mass of approximately 0.5 kg to its lower end. The wire was left in this condition for a period of typically 24 h before the lower end clamp was tightened, and finally, the excess wire protruding from each end was cut off. Tensioned in this way, the fundamental transverse resonance frequency of the wire in ambient air was approximately 1000 Hz.

Electrical connections, two to each end, were made with PTFE insulated Cu lead wires. The pair from one end passed back though the ceramic tube so that all four wires could pass out through a single electrical feedthru unit. The Monel end pieces were provided with holes so that the copper wires passing through the ceramic tube were kept well away from the vibrating wire, close to the inner diameter. The electrical feedthru (Greene-Tweed, part 5672-4592-002) was fitted in a custom tee-piece attached to the end of the tubular pressure vessel that contained the VW sensor. A junction box on the outside permitted onward connection via coaxial cables to the lock-in amplifier (Stanford Research Systems SR830).

The VW viscometer was housed within a tubular pressure vessel (Sieber-Sitec, part 740.1222) fabricated from HC-276 and rated for a maximum working pressure of 100 MPa at T = 473 K. The ends of the vessel were closed by plugs fitted with 9.53 mm diameter tube extensions and Bridgeman-style seals comprising a glass-filled PTFE sealing ring backed with Torlon antiextrusion rings, and a stainless steel trust ring. This assembly was retained by a threaded gland, and the tube adapters were connected to the fluid system to allow fluids in and out. To regulate the temperature of the VW viscometer, a heat exchanger sleeve, made from aluminum, was fitted over the outside of the pressure vessel and sealed with Viton O-rings. Silicone oil from a circulating thermostatic bath (Huber Petit-Fleur, Tango) was passed through this heat exchanger, and insulation was provided by an outer layer of silicone-rubber sponge. The temperature was measured using a platinum resistance thermometer (PRT, Sensing Devices Ltd., Ceramic Capsule PT100/1P Band 5) located in a thermowell in the wall of the pressure vessel.

The VT densimeter was an Anton Paar model DMA HPM rated for operation at temperatures from 263.15 K to 473.15 K at pressures up to 138 MPa. It was connected to an evaluation unit (mPDS 2000 V3) that served to excite oscillations of the tube at its fundamental resonance frequency and to digitize the period of oscillation. The densimeter was fitted with an internal heat exchanger through which silicone oil was passed from the circulating thermostatic bath; the densimeter and viscometer heat exchangers being connected in parallel. The temperature of the densimeter was measured using a second PRT located in a thermowell at the center of the instrument.

As shown in Figure 1, the VW and VT instruments were connected in a loop, fitted with a circulation pump, around which the fluids under study could be circulated. The purpose of the circulating pump was to permit *in situ* homogenization of the fluid mixture under study. The circulating pump was a pneumatically operated reciprocating pump similar in design to that of Peleties et al.[21] The pump cylinder was honed to an inside diameter of 5.00 mm and fitted with a piston of diameter 4.97 mm. This piston comprised a soft-iron core encapsulated in a polyphenylene sulfide (PPS) sleeve with end-caps sealed in place using epoxy resin (Stycast 2850 FT cured with catalyst 9). The pump incorporated four check valves operated in a vertical orientation such that the ceramic poppets sealed under gravity without the need for a spring. The pump was mounted on a thick aluminum plate, fitted with electrical heaters and a temperature sensor, and the whole assembly was enclosed within an insulated box. Thus, operating with a process controller, the temperature of the circulation pump could be regulated.

A set of syringe pumps (Quizix Q5000-20k) made from HC-276 were used to inject fluids into the loop. These pumps had a displacement of 5.2 cm^3 and a maximum working pressure of 138 MPa. In the present work, only one pump cylinder was used (to inject water). CO_2 was introduced directly into the system from a gas bottle fitted with a filter and pressure regulator. The pressure of the system was monitored using a pressure transducer (Honeywell model TJE) having a full-scale range of 104 MPa, located in the flow loop between the VW viscometer and VT densimeter. The pressure in the syringe pump was separately monitored using a pressure transducer installed in the head of the pump.

3. MATERIALS

The chemical samples used in this work are detailed in Table 2. The water was thoroughly degassed by agitation under vacuum prior to injection into the system.

Table 2. Description of Chemical Samples

chemical name	source	purity	additional purification
carbon dioxide	BOC	0.99995	none
water	Millipore Direct-Q UV3 apparatus	electrical resistivity > 18 MΩ·cm at T = 298 K	degassed under vacuum

dx.doi.org/10.1021/je5009125 | J. Chem. Eng. Data 2015, 60, 171−180

4. CALIBRATION PROCEDURES AND VALIDATION RESULTS

4.1. Temperature and Pressure. The Honeywell TJE pressure transducer was calibrated against a hydraulic pressure balance (DH Budenberg model 580EHX) at pressures of (20, 40, 60, 80, and 100) MPa, using both rising and falling pressure. The pressure was correlated as a linear function of the output voltage with a standard deviation of 0.02 % of reading. Sensor drift was checked by periodically comparing the measured pressure when open to the atmosphere with the reading of a digital barometer in the same laboratory and accounted for by adjusting the zero of the sensor. Taking this factor into account, the standard uncertainty of the pressure was taken to be 0.1 MPa.

The two PRTs used in the system to measure the temperatures were calibrated in a constant-temperature bath by comparison with a standard PRT which was itself calibrated on ITS-90. The calibration was performed in the temperature range (273 to 473) K at 50 K intervals; the resistance−temperature data were used to determine the constants in the Callendar−van Dusen equation. The overall standard uncertainty of the measured temperatures was estimated to be 0.025 K.

4.2. Densimeter. The period of oscillation τ of the vibrating U-tube densimeter is generally related to the density by

$$\rho(T, p) = A(T, p)\tau^2 - B(T, p) \tag{4}$$

where A and B are functions of temperature and pressure to be determined, in principle, by calibration with two reference fluids. In this work we have followed the simplified calibration procedure developed by Lagourette et al.[22] and later modified by Comuñas et al.[23] in which a single reference fluid, water, is used together with measurements under vacuum. This amounts to an assumption that A and B have the same dependence upon pressure as, applying eq 4 to the cases of water and vacuum measurements and solving for A and B, one finds:

$$A(T, p) = \frac{\rho_w(T, p)}{\tau_w^2(T, p) - \tau_0^2(T)} \tag{5}$$

and

$$B(T, p) = \frac{\rho_w(T, p)\tau_0^2(T)}{\tau_w^2(T, p) - \tau_0^2(T)} \tag{6}$$

where subscript "w" denotes water and "0" denotes vacuum. It is then sufficient to correlate A as a function of temperature and pressure and, separately, τ_0^2 as a function of temperature. In the present work, calibration measurements were made under vacuum at each nominal experimental temperature and in pure deionized water at each nominal temperature and pressure. The densities of water were obtained from the equation of state of Wagner and Pruss[24] which forms the basis of the 1995 recommendations of the International Association for the Properties of Water and Steam (IAPWS) for the thermodynamic properties of water. The results of these calibration equations were represented by the following empirical equations:

$$\tau_0^2 = \sum_{i=0}^{3} c_i (T/\mathrm{K})^i \tag{7}$$

and

$$A = \sum_{i=0}^{3}\sum_{i=0}^{1} a_{ij}(T/\mathrm{K})^i[p/(0.1\mathrm{MPa})]^j \tag{8}$$

The standard uncertainties of these correlations are 0.003 μs for τ_0 and $1.0\cdot10^{-7}$ kg·m^{-3}·μs^{-2} for A. The overall uncertainty of A is also influenced by the uncertainty of the density of the reference fluid. The relative uncertainty given by Pruss and Wagner[24] varies over the range of our measurement up to a maximum of 0.01 %. Interpreting that figure as twice the standard relative uncertainty of ρ_w, we find the overall standard uncertainty of A to be $1.6\cdot10^{-7}$ kg·m^{-3}·μs^{-2}, fractionally $6\cdot10^{-5}$. It is likely that the number of parameters in eqs 7 and 8 could have been reduced by eliminating terms of low statistical significance. However, since the calibration data set was large, and the correlations for τ_0 and A were used only as a means of interpolation, we believe that the approach adopted is robust.

Finally, the density of the fluid under study was obtained in terms of the measured period τ and the calibration equations for $A(T,p)$ and $T_0^2(T)$ as follows:

$$\rho(T, p) = A(T, p)[\tau^2 - \tau_0^2(T)] \tag{9}$$

4.3. Vibrating-Wire Sensor. In the case of the viscometer, the most important parameter determined by calibration was the mean radius R. This was obtained at a reference temperature of 296 K and at a pressure of 1 MPa by means of a calibration measurement in pure deionized water. The viscosity of water was obtained from the IAPWS recommended equation for water viscosity[25] while the density was obtained as above from the IAPWS-95 equation of state of Pruss and Wagner.[24] This led to a radius of 73.04 μm at the reference temperature. Considering the standard uncertainty in the reference value of the viscosity of water, which we take to be 0.2 %, and the repeatability of the calibration experiment, the standard relative uncertainty of R is estimated to be 0.25 %. The radius at other temperatures was calculated making use of a literature value for the mean linear expansivity of the wire material; compressibility effects were negligible. The logarithmic decrement Δ_0 was also required and was inferred from measurements in ambient air with the result $\Delta_0 = 35\cdot10^{-6}$. To validate the viscometer, additional measurements were made in pure water over the whole working range of the instrument. The results of these experiments were found to agree with the IAPWS recommended equation to within ± 1 %.

4.4. System Volume. The system volume was required in the quantitative preparation of the mixtures and was determined by the following procedure. The piston of the syringe pump was fully extended and both the fill and delivery valves were closed. The system was evacuated using a vacuum pump connected at the outlet. The temperature was controlled at 298.15 K both in the system and at the syringe pump. A sample of pure deionized water was connected to the delivery line to the syringe pump. It was degassed through agitation under vacuum until no air bubbles were visible. The delivery tube was lowered to beneath the liquid level and the sample was repressurized to ambient pressure by removing the tube to the vacuum pump. The fill valve was then opened and the piston was retracted to around four-fifths to take up the fluid. This valve was closed and the fluid in the barrel was compressed to 1 MPa. The volume of the cylinder was zeroed on the control software. The delivery valve was opened and the piston was driven forward to inject the fluid but stopped just

dx.doi.org/10.1021/je5009125 | J. Chem. Eng. Data 2015, 60, 171−180

before the end of the stroke. The delivery valve was closed, the cylinder was recompressed to 1 MPa and the volume injected was recorded. The pressure of barrel was set to 0.1 MPa and the fill valve was opened once this was reached. New fluid was taken up and this process was repeated until the system pressure reached 1 MPa, with the volume injected in each stroke being recorded. On the last stroke, the pump was set to constant pressure mode so as to control the pressure of the system. Once equilibrium was reached, the volume of the final stroke was noted. The volume of the system at 298.15 K found by this method was 44.09 cm^3. This system volume calibration was performed three times and was found to be repeatable to ± 0.01 cm^3 with an overall standard uncertainty of 0.09 cm^3, or 0.2 %·V.

5. MIXTURE PREPARATION

A sample of pure deionized water was degassed while stirring under vacuum with the delivery valve of the syringe pump closed. Meanwhile, the system was evacuated through valves V2 and V3 (see Figure 1). The temperature of the viscometer and densimeter was controlled to the temperature of the laboratory (294.15 K) to ensure isothermal filling.

CO_2 was admitted through valve V1 to an initial charging pressure of (1, 2, or 3) MPa, based on estimates of the solubility in water obtained the model by Duan et al.,[26] originally developed in ref 27. Since the VW sensor could only operate correctly in the single phase compressed liquid region, it was important not to introduce an excess of CO_2.

Water was then injected stepwise following the same procedure outlined in the calibration for the system volume, except it was injected to a pressure of typically 15 MPa. Once this pressure was reached, the mixture was homogenized using the circulating pump. The total volume injected was monitored using the syringe pump control software. It took around 3 h to achieve a homogeneous mixture. At this point, the volume of the syringe pump on the final stroke was noted to allow calculation of the amount of water injected. It was then possible to determine the mole fraction x of CO_2 in the homogeneous mixture. Measurements were performed with the pressure always above the bubble point at the experimental temperature to ensure that the system remained in the homogeneous compressed liquid region.

The standard uncertainty $u(x)$ of the mole fraction of CO_2 is related to the standard relative uncertainties $u_r(n_1)$ and $u_r(n_2)$ of the amounts n_1 and n_2 of CO_2 and water, respectively, as follows:

$$u^2(x) = [x(1 - x)]^2[u_r^2(n_1) + u_r^2(n_2)] \quad (10)$$

Since the CO_2 filling pressure was low, $u_r(n_1)$ may be related approximately to the standard relative uncertainties of pressure, temperature, and system volume by means of a perfect-gas approximation which gives

$$u_r^2(n_1) = u_r^2(p) + u_r^2(T) + u_r^2(V) \quad (11)$$

For the water, $u_r(n_2)$ may be expressed in terms of the standard uncertainties of pressure and temperature and the standard relative uncertainty of the system volume as follows:

$$u_r^2(n_2) = [\beta_T u(p)]^2 + [\alpha_p u(T)]^2 + u_r^2(V) \quad (12)$$

where α_p is the isobaric expansivity and β_T the isothermal compressibility of water. Since the parts of the system volume other than the viscometer and the densimeter were not temperature controlled, an enlarged temperature uncertainty of 1 K is ascribed to the filling condition. On the other hand, since the CO_2 filling pressure was measured immediately after rezeroing of the pressure transducer, a reduced uncertainty of 0.05 MPa was ascribed to that pressure. The terms involving α_p and β_T turn out to be entirely negligible, and the remaining terms are dominated by the pressure uncertainty in eq 11; recognizing also that $x \ll 1$, the following simple approximation for $u(x)$ suffices for practical calculations:

$$u(x) \approx x u_r(p) \quad (13)$$

This gives $u(x)$ = 0.0004 for all mixtures studied.

6. UNCERTAINTY BUDGET FOR DENSITY AND VISCOSITY

The standard uncertainties of the state variables T, p, and x have been detailed above and we now consider the uncertainties of the measured density and viscosity. Since the density is a required input in the determination of the viscosity, we consider first the overall uncertainty of the density. The standard uncertainty in the density $u(\rho)$ is associated with the standard uncertainties $u(T)$, $u(p)$, $u(x)$, and $u(\tau)$ in temperature, pressure, mole fraction, and period, respectively. Additionally, $u(\rho)$ is influenced by the uncertainties $u(\tau_0)$ and $u(A)$ of the calibration parameters τ_0 and A. These terms have been discussed above, except for the $u(\tau)$ which we take to be 0.020 μs to encompass the observed repeatability uncertainty. The uncertainty budget for density is exemplified in Table 3 for the case of the median temperature, pressure, and mole fraction. The uncertainty was found not to vary significantly over the range of conditions investigated, and the median-state standard relative uncertainty of 0.033 % was therefore ascribed to all densities.

Table 3. Uncertainty Budget for Density at the Median State Point in Terms of Standard Uncertainty $u(X)$ of Dimensionless Parameter X and Arising Contribution $u_r(\rho)$ to the Overall Standard Relative Uncertainty of Density

dimensionless parameter	value	standard uncertainty	$10^2 u_r(\rho)$
T/K	373.150	0.025	0.002
p/MPa	50.0	0.1	0.004
x	0.0170	0.0004	0.016
τ/μs	2656.18	0.020[a]	0.027
τ_o/μs	2580.58	0.003	0.004
A/(kg·m^{-3}·μs^{-2})	2.4919·10^{-3}	1.6·10^{-7}	0.006
overall combined standard relative uncertainty			0.033

[a]Includes repeatability uncertainty.

The standard uncertainty in the viscosity $u(\eta)$ is associated with the standard uncertainties of temperature, pressure, and mole fraction, and also with the standard uncertainties of the density, the wire radius, and its thermal expansivity, the vacuum decrement, and finally the repeatability uncertainty. The uncertainty budget for viscosity is exemplified in Table 4 for the case of the median temperature, pressure, and mole fraction. The two most significant terms are the uncertainties in the calibrated radius and the repeatability uncertainty. The latter was estimated from repeated check measurements on pure water to be 0.005·η. As with the density, the uncertainty of the viscosity was found to vary little over the range of conditions investigated and the median-state standard relative uncertainty of 0.7 % was therefore ascribed to all viscosities.

dx.doi.org/10.1021/je5009125 | J. Chem. Eng. Data 2015, 60, 171−180

Table 4. Uncertainty Budget for Viscosity at the Median State Point in Terms of Standard Uncertainty $u(X)$ of Dimensionless Parameter X and Arising Contribution $u_r(\eta)$ to the Overall Standard Relative Uncertainty of Viscosity

dimensionless parameter X	X	$u(X)$	$10^2 u_r(\eta)$
T/K	373.150	0.025	0.03
p/MPa	50.0	0.1	0.01
x	0.0170	0.0001	0.01
$\rho/(\mathrm{kg\cdot m^{-3}})$	986.53	0.46	0.04
R/μm	73.04	0.18	0.50
$10^6\Delta_0$	29.9	15	0.03
$\alpha_w/(10^{-6}\ \mathrm{K^{-1}})$	8.7	0.4	0.01
η/(mPa·s)	0.5778	0.0029[a]	0.50
overall combined standard relative uncertainty			0.71

[a]Repeatability uncertainty.

7. EXPERIMENTAL RESULTS AND CORRELATIONS

Measurements were performed in the temperature range (294 to 449) K for viscosity and (274 to 449) K for density, at nominal pressures of (15, 30, 50, 70 and 100) MPa, and at mole fractions of CO_2 of approximately (0.009, 0.017, and 0.027). The state points selected for measurements were guided by the solubility model of Duan et al.[26,27] and chosen such that the mixture remained in a single-phase state. As a consequence, some combinations of temperature, pressure, and mole fraction implied by the ranges above were avoided. Although the apparatus was designed for simultaneous measurements of density and viscosity, the present results for these two properties were actually obtained in separate experiments.

7.1. Density. The density results are given in Table 5. The approximate overall relative standard uncertainty in density across all points is 0.4 $\mathrm{kg\cdot m^{-3}}$. The data show a linear dependence upon x at constant T and p as illustrated in Figure 2 panels a and b for low and high temperature, respectively. To analyze the data further, the molar volume V_m of the solution is considered and, as shown in Figure 3 (for an example pressure of 70 MPa), this too is a linear function of x. Similar behavior is observed at each temperature, and pressure and we therefore assume that the partial molar volumes of H_2O (V_w) and of CO_2 (V_{CO2}) are independent of x within the range investigated and we correlated the data at each T and p as follows:

$$V_m = Ax + B \tag{14}$$

To constrain the correlation at $x = 0$, the experimental data were augmented by values of the molar volume of pure water at each experimental temperature and pressure calculated from the IAPWS-95 equation of state. Thus, at the majority of temperatures and pressures, four values of the molar volume were used to determine the two parameters in eq 14 by means of a linear regression.

In terms of the parameters in eq 14, the partial molar volume of CO_2 is given by

$$V_{CO_2} = V_m + (1 - x)(\partial V_m/\partial x)_{T,p} = A + B \tag{15}$$

The standard uncertainty of V_{CO_2} determined in this way was, on average, 0.15 $\mathrm{cm^3\cdot mol^{-1}}$. Equation 14 also gives the molar volume of the solvent (pure water), $V_w = B$. Figure 4 shows V_{CO_2} as a function of temperature along each isobar and, from this, a six parameter correlation has been established for $V_{CO_2}(T, p)$ that is linear in pressure and quadratic in temperature as follows:

$$V_{CO_2}/(\mathrm{cm^3\cdot mol^{-1}}) = \sum_{i=0}^{2}\sum_{j=0}^{1} a_{ij}(T/\mathrm{K})^i(p/\mathrm{MPa})^j \tag{16}$$

Table 5. Experimental Densities ρ of $[(1 - x)H_2O + xCO_2]$ at Temperatures T and Pressures p[a]

p/MPa	$\rho/(\mathrm{kg\cdot m^{-3}})$	p/MPa	$\rho/(\mathrm{kg\cdot m^{-3}})$	p/MPa	$\rho/(\mathrm{kg\cdot m^{-3}})$
			x = 0.0086		
T = 274.73 K		T = 296.17 K		T = 323.45 K	
15.01	1012.0	15.10	1008.6	15.02	998.4
30.11	1019.0	30.20	1015.0	30.13	1004.7
50.24	1028.1	50.26	1023.4	50.25	1012.8
70.36	1036.8	70.33	1031.4	70.36	1020.6
100.67	1049.3	100.65	1042.9	100.72	1031.6
T = 348.32 K		T = 373.42 K		T = 398.55 K	
15.05	984.8	15.09	967.8	15.06	948.3
30.15	991.3	30.18	974.6	30.17	955.6
50.27	999.5	50.28	983.2	50.29	964.9
70.37	1007.3	70.39	991.5	70.39	973.7
100.71	1018.6	100.71	1003.2	100.71	986.0
T = 423.92 K		T = 449.20 K			
15.07	925.9	15.08	900.7		
30.18	934.0	30.19	909.9		
50.30	944.2	50.31	921.3		
70.42	953.8	70.42	931.8		
100.71	967.1	100.71	946.4		
			x = 0.0168		
T = 274.77 K		T = 296.19 K		T = 323.43 K	
15.08	1017.3	15.07	1013.3	15.06	1002.5
30.19	1024.1	30.17	1019.7	30.18	1008.8
50.31	1033.0	50.30	1027.9	50.30	1016.9
70.43	1041.6	70.41	1035.9	70.42	1024.6
100.71	1053.9	100.73	1047.3	100.72	1035.7
T = 348.38 K		T = 373.46 K		T = 398.55 K	
30.20	994.9	30.19	977.8	30.19	958.2
50.32	1003.2	50.32	986.5	50.33	967.8
70.45	1011.1	70.45	994.9	70.46	976.7
100.74	1022.4	100.74	1006.7	100.73	989.4
T = 423.93 K		T = 449.20 K			
30.20	935.7	30.21	910.8		
50.34	946.2	50.36	922.6		
70.46	956.0	70.47	933.5		
100.73	969.7	100.74	948.4		
			x = 0.0271		
T = 274.72 K		T = 296.18 K		T = 323.43 K	
30.29	1030.1	30.25	1025.3	70.46	1029.6
50.41	1038.8	50.36	1033.4	100.78	1040.7
70.53	1047.2	70.44	1041.2		
100.77	1059.2	100.76	1052.6		
T = 348.33 K		T = 373.38 K		T = 398.48 K	
70.58	1015.3	70.59	998.2	50.47	970.0
100.78	1026.8	100.80	1010.3	70.60	979.3
				100.80	992.1
T = 423.84 K		T = 449.17 K			
50.46	948.0	50.45	923.6		
70.58	958.1	70.57	934.9		
100.81	972.1	100.80	950.3		

[a]Standard uncertainties are $u(T)$ = 0.025 K, $u(p)$ = 0.1 MPa, and $u(\rho) = 0.00033\cdot\rho$.

dx.doi.org/10.1021/je5009125 | J. Chem. Eng. Data 2015, 60, 171−180

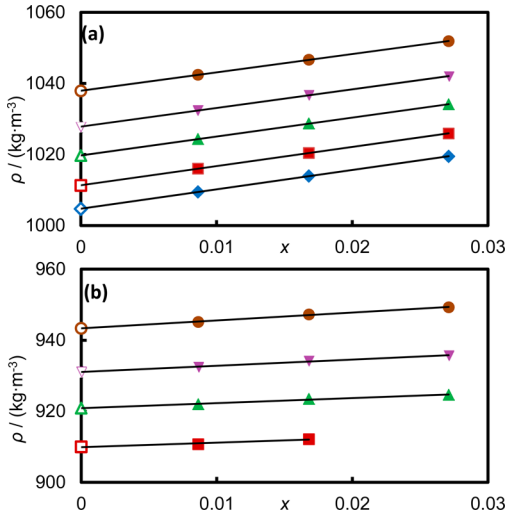

Figure 2. Densities ρ of $[(1 - x)H_2O + xCO_2]$ as a function of x at (a) T = 296 K and (b) T = 449 K. Experimental data: ◆, 15 MPa; ■, 30 MPa; ▲, 50 MPa; ▼, 70 MPa, ●, 100 MPa. Open symbols at x = 0 are calculated from the IAPWS-95 equation of state.[24] Solid lines are linear regression lines.

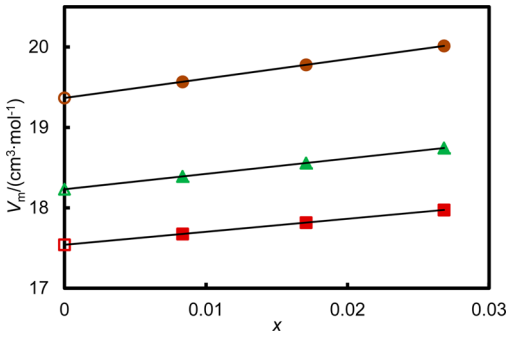

Figure 3. Molar volume V_m of $[(1 - x)H_2O + xCO_2]$ as a function of x at p = 70 MPa. Experimental data: ■, 296 K; ▲, 373 K; ●, 449 K. Open symbols at x = 0 are calculated from IAPWS-95 equation of state.[24] Solid lines are linear regression lines.

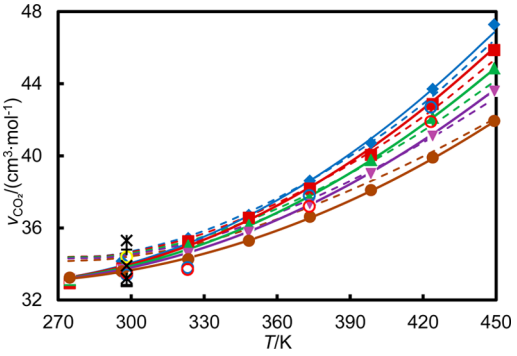

Figure 4. Partial molar volume V_{CO2} of CO_2 in aqueous solution as a function of temperature T. This work: ◆, 15 MPa; ■, 30 MPa; ▲, 50 MPa; ▼, 70 MPa, ●, 100 MPa. Literature data at p > 0.1 MPa: ○, Hněkovský et al.[28] at pressures of 1 MPa (yellow), 20 MPa (blue), and 35 MPa (red). Literature data at p = 0.1 MPa: −, Barbero et al.;[31] ×, Moore et al.;[29] +, Enns et al.;[30] and ∗, Ellis et al.[34] Solid lines and dashed lines represent eq 16 and the model of Sedlbauer et al.,[32] respectively, at pressures (from the top down) of (15, 30, 50, 70, and 100) MPa.

The values for the coefficients are given in Table 6 and the standard uncertainty of the correlation is 0.16 $cm^3 \cdot mol^{-1}$. The final model for the density of a mixture $\rho(T, p, x)$ is based on the IAPWS-95 EOS for the molar volume of pure water[24] and eq 16 for the partial molar volume of CO_2 as follows:

$$\rho = \frac{xM_{CO_2} + (1 - x)M_w}{xV_{CO_2} + (1 - x)V_w} \quad (17)$$

Figure 4 shows that V_{CO_2} increases in magnitude and becomes more dependent upon pressure with increasing temperature. Also shown in Figure 4 are data and models from the literature,[28−32] and it can be seen that there is a fair degree of agreement. In particular, the model of Sedlbauer et al.[32] is in very close agreement with the present data at temperatures between (323 and 423) K at pressures up to 70 MPa. At other temperatures, and also at the highest pressure, some deviations are apparent. At 274 K, the model of Sedlbauer et al. is about 1 $cm^3 \cdot mol^{-1}$ greater than eq 16.

In Figure 5, we compare our experimental densities, along with data from the literature,[10,13,33] with our model (eqs 16 and 17) as functions of x, T, and p. The model represents all of the present experimental data within ± 0.04 %, and the deviations do not depend systematically on any of the three independent variables. The experimental values plotted at x = 0 are derived from the values of B in eq 14, determined at each experimental temperature and pressure. King et al.[33] performed measurements in the temperature range (288 to 313) K at pressures up to around 20 MPa with a claimed uncertainty of 0.5 %. From Figure 5, we see that these data agree with the present model to within ± 0.25 %. Hebach et al.[13] determined densities using a calibrated vibrating tube densimeter with a claimed uncertainty of 0.15 % at temperatures from (284 to 332) K and pressures up to 30 MPa; their data agree with the present model mostly to within ± 0.2 %. Li et al.[10] reports measurements performed with a PVT apparatus coupled to a densimeter in a pressure range of (0.3 to 29) MPa at a single temperature of 332 K, and the maximum uncertainty in density was claimed to be 0.1 $kg \cdot m^{-3}$, or about 0.01 %. However, from Figure 5, we see that there are deviations of up to 0.4 % from our correlation.

7.2. Viscosity. The viscosity results are given in Table 7. The determination of viscosity with the VW viscometer requires knowledge of the fluid density and the values used were those obtained in the present study. The viscosity data show a linear dependence upon both pressure and the mole fraction x of dissolved CO_2. The dependence of the viscosity upon mole fraction x at constant T and p is illustrated in Figures 6 panels a and b for low and high temperature, respectively, and it can be seen that the effect is more pronounced at low temperature. Here, increasing the CO_2 concentration to near saturation increases the viscosity of the mixture by about 10 % from that of pure water. However, at the highest temperature studied the relative effect is just over 1 %. The dependence of the viscosity upon pressure at constant T and x was also observed to be linear to within the experimental uncertainty.

For practical applications, a correlation of the data is desirable. To constrain the correlation at x = 0, the experimental data were augmented by values of the viscosity of pure liquid water computed from the IAPWS recommended equation for water viscosity[25] at each experimental temperature and pressure. Additionally, calculated data were added at T = 274 K and each experimental pressure.

dx.doi.org/10.1021/je5009125 | J. Chem. Eng. Data 2015, 60, 171−180

Table 6. Coefficients of eq 16 for the Partial Molar Volume of CO_2 in Aqueous Solution

$a_{0,0}$	$a_{1,0}$	$a_{2,0}$	$a_{0,1}$	$a_{1,1}$	$a_{2,1}$
51.19	−0.15575	$3.2955\cdot10^{-4}$	$-6.0708\cdot10^{-2}$	$5.5026\cdot10^{-4}$	$-1.2114\cdot10^{-6}$

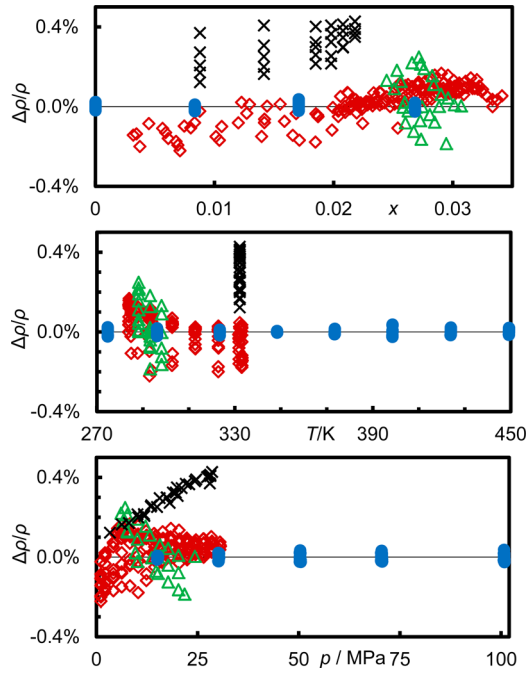

Figure 5. Deviations $\Delta\rho = (\rho_{exp} - \rho_{calc})$ between experimental densities ρ_{exp} of $[(1 - x)H_2O + xCO_2]$ and densities ρ_{calc} calculated from eqs 16 and 17 with the IAPWS-95 equation of state for the density of pure water:[24] ●, this work; ◇ Hebach et al.;[13] △, King et al.;[33] and ×, Li et al.[10]

Motivated by the observed dependence upon p and x, a correlation of the form

$$\ln \eta = \ln \eta_0 + f_1 x + f_2 p \tag{18}$$

was tested in which η_0 represents the viscosity of the hypothetical pure liquid water at temperature T and p = 0, and f_1 and f_2 are functions of temperature only. Figure 7 shows the values of η_0, f_1, and f_2 obtained from analysis of the data at each temperature. It was found that f_1 decreased exponentially with increasing temperature, while f_2 could be represented as a linear function of inverse temperature. Accordingly, the following modified Vogel–Fulcher–Tamman (VFT) equation was used to correlate the data:

$$\ln[\eta/(\text{mPa·s})] = a + b(p/p_0) + \frac{c + d(p/p_0)}{(T/T_0 - 1)} + e_1 \exp[-e_2(T/T_0 - 1)]x \tag{19}$$

Here, p_0 = 1 MPa, and a, b, c, d, e_1, e_2, and T_0 are parameters. This form of this equation (without the fourth term) is used extensively for modeling the effects of temperature and pressure on viscosity. Three of the seven parameters (a, c, and T_0) describe the viscosity of pure liquid water as a function of temperature at p = 0, two of them (b and d) describe the dependence upon pressure, and the remaining two are required to account for the dissolved CO_2. The parameters of the model were fitted to the augmented data set using an objective function based on the absolute average relative deviation, defined by

Table 7. Experimental Viscosities η of $[(1 - x)H_2O + xCO_2]$ at Temperatures T and Pressures p[a]

p/MPa	η/(mPa·s)	p/MPa	η/(mPa·s)	p/MPa	η/(mPa·s)
			x = 0.0086		
T = 294.30 K		T = 322.93 K		T = 373.13 K	
15.1	1.013	15.0	0.560	15.0	0.286
30.2	1.014	30.1	0.564	30.1	0.291
50.3	1.012	50.2	0.568	50.2	0.297
70.3	1.008	70.2	0.573	70.3	0.302
96.4	1.008	96.3	0.582	96.4	0.308
T = 397.98 K		T = 424.03 K		T = 448.93 K	
30.1	0.231	30.1	0.190	30.0	0.162
50.2	0.236	50.2	0.194	50.1	0.167
70.3	0.242	70.2	0.199	70.2	0.172
96.4	0.248	96.4	0.205	96.3	0.178
			x = 0.0168		
T = 294.27 K		T = 322.91 K		T = 373.03 K	
15.1	1.049	15.0	0.568	30.1	0.2932
30.2	1.044	30.1	0.573	50.2	0.2989
50.2	1.044	50.2	0.578	70.2	0.3040
70.2	1.041	70.2	0.584	96.2	0.3111
96.3	1.046	96.2	0.592		
T = 397.88 K		T = 422.91 K		T = 448.29 K	
30.1	0.233	30.0	0.192	30.0	0.163
50.2	0.238	50.1	0.196	50.1	0.168
70.2	0.244	70.2	0.202	70.1	0.173
96.3	0.250	96.2	0.208	96.2	0.179
			x = 0.0271		
T = 294.31 K		T = 323.12 K		T = 374.09 K	
30.3	1.096	70.4	0.606	70.3	0.309
50.3	1.095	96.5	0.615	96.4	0.318
70.4	1.097				
96.5	1.100				
T = 398.98 K		T = 423.82 K		T = 448.71 K	
50.2	0.241	50.2	0.198	50.2	0.169
70.2	0.245	70.3	0.204	70.2	0.173
96.3	0.254	96.5	0.210	96.4	0.179

[a]Standard uncertainties are $u(T)$ = 0.025 K, $u(p)$ = 0.1 MPa, and $u(\eta)$ = 0.007·η.

$$\Delta_{AAD} = \frac{1}{N}\sum_{i=1}^{N}\left(\frac{|\eta_i - \eta_{i,fit}|}{\eta_i}\right) \tag{20}$$

Here, η_i is an experimental datum, $\eta_{i,fit}$ is calculated from the correlation applied at the same state point, and N is the total number of points. This resulted in the parameters reported in Table 8. The absolute average relative deviation for the fit was 0.4 %, while the maximum absolute relative deviation was 1.7 %.

In Figure 8, we plot the deviations of the present data from the surface-fit correlation. It can be noticed that the present model applied at x = 0 agrees closely with the IAPWS recommended viscosity equation.[25] In fact, except at T < 278 K the agreement is well with ± 1 %; the absolute relative deviation between eq 19 and the IAPWS formulation increase somewhat near the triple point where it reaches a maximum of 1.7 %. Also shown in Figure 8 are the measurements reported

dx.doi.org/10.1021/je5009125 | J. Chem. Eng. Data 2015, 60, 171−180

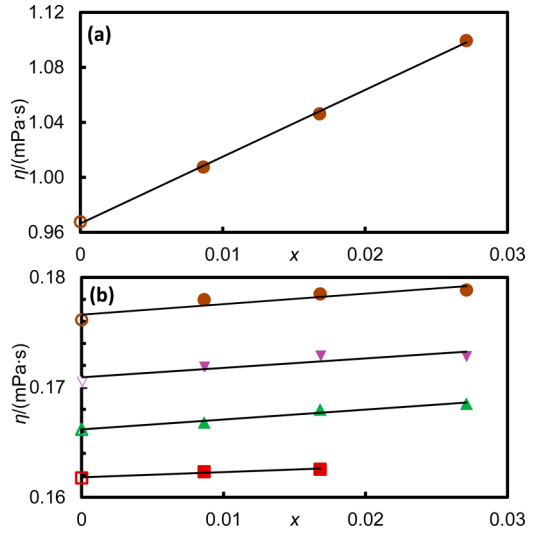

Figure 6. Viscosities η of $[(1 - x)\ H_2O + x\ CO_2]$ as a function of x at (a) T = 296 K and (b) T = 449 K. Experimental data: ■, 30 MPa; ▲, 50 MPa; ▼, 70 MPa, ●, 96 MPa. Open symbols at x = 0 are calculated from the IAPWS-95 equation for water viscosity.[25] Solid lines are linear regression lines.

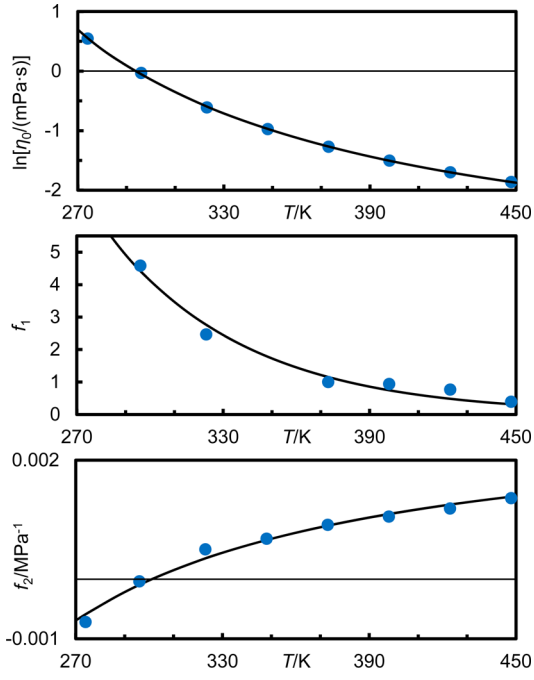

Figure 7. Parameters η_0, f_1, and f_2 determined with eq 18 from the experimental viscosities of $[(1 - x)H_2O + xCO_2]$ at temperatures T: ●, isothermal fits; ———, surface fit.

by Kumagai et al.[11] which agree with the correlation to within ± 2 %. These data were gathered at temperatures of (273.15 to 278.1) K and the good agreement observed validates the present model for application at temperatures down to 273.15 K. It should be noted that there exists a second literature data set, not shown in Figure 8: that of Uchida et al.[12] based on

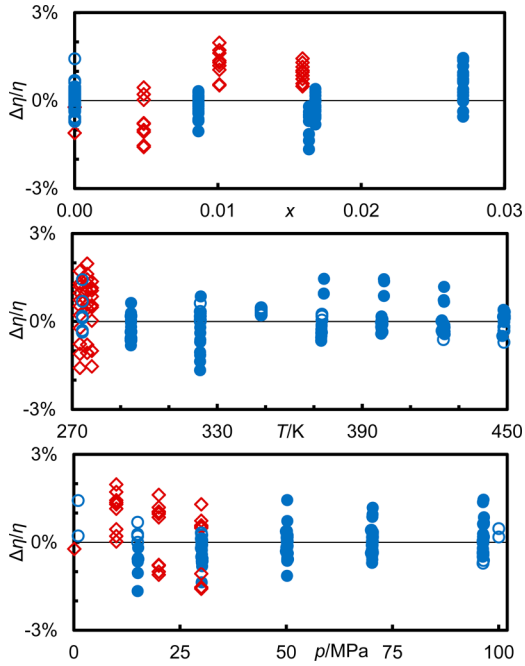

Figure 8. Deviations $\Delta\eta = (\eta_{exp} - \eta_{calc})$ between experimental viscosities η_{exp} of $[(1 - x)H_2O + xCO_2]$ and viscosities η_{calc} calculated from eq 19: ●, this work; ○, pure water from IAPWS equation;[25] ◇, Kumagai et al.[11]

dynamic light scattering experiments on saturated solutions at pressures of (0.7 and 5.0) MPa. Unfortunately, these data have a relative uncertainty of about 6 % which is too large to resolve the effect of dissolved CO_2 at the lower pressure investigated. Furthermore, the data at the higher pressure were gathered in states at which CO_2 hydrates are stable; these showed a strong dependence upon time and deviate from the present model by as much as 40 %.

8. CONCLUSION

Experimental and modeling results are reported for the density and viscosity of pure water with known mole fractions of dissolved CO_2. The density model is based on the partial molar volume for CO_2 in aqueous solution. This quantity has been correlated from (274 to 449) K and from the bubble pressure to p = 100 MPa. When combined with the IAPWS-95 equation of state of pure water, this correlation represents the measured densities of undersaturated solutions of CO_2 in water within ± 0.04 %

The modified Vogel–Fulcher–Tamman equation was used to correlate the viscosity as a function of temperature, pressure, and mole fraction of CO_2 with an absolute average relative deviation of 0.4 %. This model is valid from (273 to 449) K and from the bubble pressure to p = 100 MPa. At x = 0, the model is in good agreement with the IAPWS recommended equation for water viscosity.

Combined with the model of Duan et al.[26,27] for CO_2 solubility, we have a complete model for the density and

Table 8. Parameters in eq 19 for the Viscosity of $[(1 - x)H_2O + xCO_2]$

a	c	b	d	e_1	e_2	T_0/K
−3.705013	3.98950	0.00289258	−0.00326	65.55968	2.46811	141.5

dx.doi.org/10.1021/je5009125 | J. Chem. Eng. Data 2015, 60, 171−180

viscosity of both saturated and undersaturated solutions of CO_2 in water.

AUTHOR INFORMATION

Corresponding Author

*E-mail: m.trusler@imperial.ac.uk.

Funding

This work was carried out as part of the Qatar Carbonates and Carbon Storage research Centre (QCCSRC). The authors gratefully acknowledge the funding of QCCSRC provided jointly by Qatar Petroleum, Shell, and the Qatar Science & Technology Park and their support of the present project and the permission to publish this research.

Notes

The authors declare no competing financial interest.

REFERENCES

(1) Houghton, J. T.; Ding, Y.; Griggs, D. J.; Noguer, M.; Linden, P. J. v. d.; Dai, X.; Maskell, K.; Johnson, C. A. *Climate Change 2001: The Scientific Basis*; Cambridge University Press: Cambridge, UK, 2001.

(2) Tabasinejad, F.; Barzin, S. Y.; Moore, G. R.; Mehta, S. A.; Fraassen, K. C. V.; Rushing, J. A.; Newsham, K. E., Water/CO_2 system at high pressure and temperature conditions: Measurement and modeling of density in equilibrium liquid and vapor phases. SPE EUROPEC/EAGE Annual Conference and Exhibition, Barcelona, Spain, 2010.

(3) Advanced Resources Int. *Optimization of CO_2 Storage in CO_2 Enhanced Oil Recovery Projects*; Office of Carbon Capture and Storage (OCCS): London, 2010.

(4) Koottungal, L. Special Report: EOR/Heavy Oil Survey: 2010 Worldwide EOR Survey. *Oil Gas J.* **2010**, *108*, 47−59.

(5) Perrin, J.-C.; Benson, S. An experimental study on the influence of sub-core scale heterogeneities on CO_2 distribution in reservoir rocks. *Transp. Porous Media* **2010**, *82*, 93−109.

(6) Saadatpoor, E.; Bryant, S.; Sepehrnoori, K. New trapping mechanism in carbon sequestration. *Transp. Porous Media* **2010**, *82*, 3−17.

(7) McMillan, B.; Navanit, K.; Bryant, S. CO_2 injectivity into brine aquifers: Why relative permeability matters as much as absolute permeability. *Energy Procedia* **2009**, *1*, 3091−3098.

(8) Patel, P. D.; Christman, P. G.; Gardner, J. W. Investigation of unexpectedly low field-observed fluid mobilities during some CO_2 tertiary floods. *SPE Reservoir Eng.* **1987**, *2*, 507−513.

(9) G. S, H.; Pau, J. B.; B, K.; Pruess, A. S.; Almgren, M. J.; Lijewski, K. Zhang High resolution simulation and characterization of density-driven flow in CO_2 storage in saline aquifers. *Adv. Wat. Resour.* **2010**, *33*, 443−455.

(10) Li, Z.; Dong, M.; Li, S.; Dai, L. Densities and solubilities for binary systems of carbon dioxide + water and carbon dioxide + brine at 59 °C and pressures to 29 MPa. *J. Chem. Eng. Data* **2004**, *49*, 1026−1031.

(11) Kumagai, A.; Yokoyama, C. Viscosity of aqueous solutions of CO_2 at high pressures. *Int. J. Thermophys* **1998**, *19*, 1315−1323.

(12) Uchida, T.; Ohmura, R.; Nagao, J.; Takeya, S.; Ebinuma, T.; Narita, H. Viscosity of aqueous CO_2 solutions measured by dynamic light scattering. *J. Chem. Eng. Data* **2003**, *48*, 1225−1229.

(13) Hebach, A.; Oberhof, A.; Dahmen, N. Density of water + carbon dioxide at elevated pressures: Measurements and correlation. *J. Chem. Eng. Data* **2004**, *49*, 950−953.

(14) Yaginuma, R.; Sato, Y.; Kodama, D.; Tanaka, H.; Kato, M. Saturated densities of carbon dioxide + water mixture at 304.1 K and pressures to 10 MPa. *Nippon Enerugi Gakkaishi* **2000**, *79*, 144−146.

(15) *Haynes Properties Manual, Hastelloy C-276 Alloy*; Haynes, Int.: Kokomo, Ind., 2001; http://www.haynesintl.com/hastelloyc276alloy/hastelloyc276alloypf.htm.

(16) Shimizu, Y.; Sasaki, T.; Kodaira, T.; Kawaguchi, K.; Terashima, K.; Koshizaki, N. Effect of plasma conditions on fabrication of multi-walled carbon nanotubes grown perpendicularly on Hastelloy C276 (R). *Diamond Relat. Mater.* **2005**, *14*, 11−15.

(17) Ciotta, F.; Maitland, G.; Smietana, M.; Trusler, J. P. M.; Vesovic, V. Viscosity and density of carbon dioxide + 2,6,10,15,19,23-hexamethyltetracosane (squalane). *J. Chem. Eng. Data* **2009**, *54*, 2436−2443.

(18) Retsina, T.; Richardson, S. M.; Wakeham, W. A. The theory of a vibrating-rod viscometer. *Appl. Sci. Res.* **1987**, *43*, 325−346.

(19) The PGM Database: Platinum - 10.00 % Iridium. http://www.pgmdatabase.com/jmpgm/index.jsp?record=1064 (accessed Sept. 30, 2014).

(20) Peleties, F.; Trusler, J. P. M. Viscosity of liquid di-isodecyl phthalate at temperatures between (274 and 373) K and at pressures up to 140 MPa. *J. Chem. Eng. Data* **2011**, *56*, 2236−2241.

(21) Peleties, F.; Trusler, J. P. M.; Goodwin, A.; Maitland, G. C. Circulating pump for high-pressure and high-temperature applications. *Rev. Sci. Instrum.* **2005**, *76*, 105103.

(22) Lagourette, B.; Boned, C.; Saintguirons, H.; Xans, P.; Zhou, H. Densimeter calibration method versus temperature and pressure. *Meas. Sci. Technol.* **1992**, *3*, 699−703.

(23) Comuñas, M. J. P.; Bazile, J. P.; Baylaucq, A.; Boned, C. Density of diethyl adipate using a new vibrating tube densimeter from (293.15 to 403.15) K and up to 140 MPa. Calibration and measurements. *J. Chem. Eng. Data* **2008**, *53*, 986−994.

(24) Wagner, W.; Pruss, A. The IAPWS formulation 1995 for the thermodynamic properties of ordinary water substance for general and scientific use. *J. Phys. Chem. Ref. Data* **2002**, *31*, 387−535.

(25) Huber, M. L.; Perkins, R. A.; Laesecke, A.; Friend, D. G.; Sengers, J. V.; Assael, M. J.; Metaxa, I. N.; Vogel, E.; Mares, R.; Miyagawa, K. New international formulation for the viscosity of H_2O. *J. Phys. Chem. Ref. Data* **2009**, *38*, 101−125.

(26) Duan, Z.; M?ller, N.; Weare, J. H. A high temperature equation of state for the H_2O−$CaCl_2$ and H_2O−MgC_{l2} systems. *Geochim. Cosmochim. Acta* **2006**, *70*, 3765−3777.

(27) Duan, Z. H.; Sun, R. An improved model calculating CO_2 solubility in pure water and aqueous NaCl solutions from 273 to 533 K and from 0 to 2000 bar. *Chem. Geol.* **2003**, *193*, 257−271.

(28) Hnedkovsky, L.; Wood, R. H.; Majer, V. Volumes of aqueous solutions of CH_4, CO_2, H_2S, and NH_3 at temperatures from 298.15 to 705 K and pressures to 35 MPa. *J. Chem. Thermodyn.* **1996**, *28*, 125−142.

(29) Moore, J. C.; Battino, R.; Rettich, T. R.; Handa, Y. P.; Wilhelm, E. Partial molar volumes of gases at infinite dilution in water at 298.15 K. *J. Chem. Eng. Data* **1982**, *27*, 22−24.

(30) Enns, T.; Scholander, P. F.; Bradstreet, E. D. Effect of hydrostatic pressure on gases dissolved in water. *J. Phys. Chem.* **1965**, *69*, 389−391.

(31) Barbero, J. A.; Hepler, L. G.; McCurdy, K. G.; Tremaine, P. R. Thermodynamics of aqueous carbon dioxide and sulfur dioxide—Heat-capacities, volumes, and the temperature-dependence of ionization. *Can. J. Chem.* **1983**, *61*, 2509−2519.

(32) Sedlbauer, J.; O'Connell, J. P.; Wood, R. H. A new equation of state for correlation and prediction of standard molal thermodynamic properties of aqueous species at high temperatures and pressures. *Chem. Geol.* **2000**, *163*, 43−63.

(33) King, M. B.; Mubarak, A.; Kim, J. D.; Bott, T. R. The mutual solubilities of water with supercritical and liquid carbon dioxide. *J. Supercrit. Fluids* **1992**, *5*, 296−302.

(34) Ellis, A. J.; McFadden, I. M. Partial molal volumes of ions in hydrothermal solutions. *Geochim. Cosmochim. Acta* **1972**, *36*, 413−426.